Research Square

Preprints are preliminary reports that have not undergone peer review.
They should not be considered conclusive, used to inform clinical practice,
or referenced by the media as validated information.

Dust–Ion Acoustic Solitons and Shocks in a Four-Component Electronegative Dusty Plasma with Warm Adiabatic Ions and Nonthermal Electrons

M. Masum Haider

masum.phy@mbstu.ac.bd

Mawlana Bhashani Science and Technology University

Obaydur Rahman

Mawlana Bhashani Science and Technology University

Md. Abdus Salam

Mawlana Bhashani Science and Technology University

Research Article

Keywords: Dusty plasma, dust-ion acoustic waves, KdV equation, KdV-Burgers equation, nonthermal electrons, solitary waves, shock waves

Posted Date: July 29th, 2026

DOI: https://doi.org/10.21203/rs.3.rs-10361407/v1

License: This work is licensed under a Creative Commons Attribution 4.0 International License.
Read Full License

Additional Declarations: No competing interests reported.

Dust–Ion Acoustic Solitons and Shocks in a Four-Component Electronegative Dusty Plasma with Warm Adiabatic Ions and Nonthermal Electrons

M. Masum Haider[1],* Obaydur Rahman[1], and Md. Abdus Salam[2]
[1] *Department of Physics, Mawlana Bhashani Science and Technology University,Santosh, Tangail-1902, Bangladesh and*
[2] *Department of Mathematics, Mawlana Bhashani Science and Technology University,Santosh, Tangail-1902, Bangladesh*
(Dated: July 18, 2026)

Nonlinear electrostatic structures in dusty plasmas are strongly modified when additional charged species and non-Maxwellian electrons are present, as occurs in laboratory SF_6-argon systems and in space environments such as Earth's mesosphere and Saturn's E-ring. This work theoretically investigates dust–ion acoustic (DIA) solitary and shock waves in an unmagnetized, collisionless electronegative dusty plasma composed of warm adiabatic positive ions, cold negative ions, Cairns-distributed nonthermal electrons, and stationary negatively charged dust grains. Using the reductive perturbation method, the Korteweg–de Vries (KdV) equation is derived for the nondissipative limit and the Korteweg–de Vries–Burgers (KdV-B) equation when ion viscosity is included. This yields analytical expressions for the DIA phase speed, nonlinear, dispersive, and dissipative coefficients, as well as their dependence on the nonthermal parameter, negative-ion concentration, dust concentration, ion mass ratio, and positive to negative ion temperature ratio. Numerical analysis shows that the phase velocity increases electron nonthermality, negative-ion concentration, and higher positive-ion temperature whereas decreased with dust content. Lighter positive ions and lower negative-ion concentration can narrow structures and induce a polarity change, whereas warmer positive ions produce shorter and wider solitons. For shock structures, viscosity induces a transition from oscillatory to monotonic profiles, controlled by the ratio of dissipation to dispersion. The dissipative coefficient scales linearly with viscosity, with a composition-dependent slope, suggesting an observational method to infer plasma composition from shock thickness. The model provides a unified framework for interpreting DIA solitary and shock structures in electronegative dusty plasmas.

Keywords: Dusty plasma; dust-ion acoustic waves; KdV equation; KdV-Burgers equation; nonthermal electrons; solitary waves; shock waves

I. INTRODUCTION

Dusty plasmas are typical electron-ion plasmas mixed with tiny solid particles ranging from micron to submicron sizes. These are found throughout space and laboratory, including planetary rings, comet tails, interstellar space, Earth's mesosphere, and industrial plasma reactors [1–4]. The charged dust particles create new wave modes that are not observed in regular two-component plasmas. Among these, dust-acoustic (DA) and dust-ion acoustic (DIA) waves are especially important [1, 2, 5]. The DIA mode derives its phase speed from the electron thermal pressure, its restoring force from electron Debye shielding, and its inertia from the ion mass. The dust particles act as a stationary negative-charge background, altering the charge neutrality condition and thus affecting the dispersion relationship [6, 7].

In the absence of dissipation, the nonlinear steepening of DIA waves leads to solitary waves, which are described by the Korteweg–de Vries (KdV) equation [8, 9]. When ion viscosity is present, the balance between nonlinearity and dissipation creates shock structures, described by the Korteweg–de Vries–Burgers (KdV-B) equation [10, 11]. The type of these nonlinear structures—compressive (positive potential) or rarefactive (negative potential)—depends on the sign of the nonlinear coefficient A in the KdV or KdV-B equation. When A = 0, it marks a critical point where the usual KdV description fails, and more complex equations like the modified KdV or the Gardner equation are needed [7, 12].

In many laboratory and space environments, plasmas consist of both positive and negative ions. Fluorine- or oxygen-based discharges frequently generate negative ions such as (F^-, O^-, SF_6^-), along with positive ions, creating electronegative plasmas [13, 14]. In space, negative ions have been observed in Titan's ionosphere [5]and in the vicinity of comets. The presence of these negative ions alters the plasma's inertia and introduces an additional acoustic mode. Research on DIA solitary waves in plasmas containing both ion types indicates that negative ions can significantly change the soliton's amplitude, width, and polarity [6, 7, 11, 15–17].

The velocity distribution functions observed in auroral acceleration regions, Saturn's magnetosphere, and cometary environments show a high-energy population that does not match a pure Maxwellian. Cairns *et al.* [18] proposed a nonthermal distribution that is widely used to model energetic electron populations. The Cairns distribution becomes a Maxwellian distribution when $\alpha = 0$ and shows a more noticeable high-energy tail as the nonthermal parameter α increases. Several studies have included Cairns distributed electrons in dusty plasma models, showing that electron nonthermality significantly changes the KdV nonlinear coefficient, alters the polar-

* masum.phy@mbstu.ac.bd

ity reversal boundary, and affects the width of solitary structures [7, 11, 12, 18–22].

DIA waves have by now been studied in numerous plasma configurations [6, 7, 11, 15, 16, 23, 24], yet a systematic treatment combining four distinct species—warm adiabatic positive ions, cold negative ions, Cairns-distributed nonthermal electrons, and a stationary charged-dust background—within a single KdV-B framework has, to our knowledge, not been reported. Bringing these four ingredients together generates a genuinely multidimensional parameter space, in which compressive, rarefactive, oscillatory, and monotonic structures can all be realized depending on where the plasma sits within that space.

The model developed here is directly relevant to several physical settings. Electronegative discharges in SF_6-based laboratory mixtures generate negative ions and have been shown to support both DIA solitons and shock-like structures [13, 14]. Satellite measurements in the mesosphere and lower ionosphere likewise reveal the simultaneous presence of charged dust, negative ions, and nonthermal electrons [5], while Cassini data from Saturn's E-ring and Titan's upper atmosphere point to comparable conditions, with negative ions coexisting alongside energetic electron populations [12]. Locating the polarity-reversal surface $A = 0$ and mapping out the compressive and rarefactive soliton regions therefore gives a practical means of interpreting wave polarity from in-situ or laboratory measurements. The transition between oscillatory and steady shock profiles with increasing ion viscosity, already documented in the controlled experiments of Nakamura *et al.* [10], can similarly be placed within the present theoretical picture.

The remainder of the paper proceeds as follows. Section II introduces the plasma model and the governing fluid equations. Section III derives the KdV equation through the reductive perturbation method and its solution. Section IV presents the derivation of KdB-Burger (KdV-B) equation with its solution. Section V discusses the numerical results, and Section VI summarizes the main conclusions.

II. PLASMA MODEL AND GOVERNING EQUATIONS

We have considered an unmagnetized, collisionless dusty plasma consisting of four species: (i) warm positive ions of mass m_p, charge $+e$, equilibrium number density n_{p0}, and temperature T_p; (ii) cold negative ions of mass m_n, charge $-Z_n e$, and equilibrium number density n_{n0} with Z_n is the ion charge number; (iii) nonthermal electrons described by the Cairns distribution [18] with temperature T_e and equilibrium density n_{e0}; and (iv) immobile negatively charged dust grains with charge $-Z_d e$ and equilibrium density n_{d0} considering Z_d as the dust charge number.

The equilibrium charge-neutrality condition reads

$$n_{p0} = n_{e0} + Z_n n_{n0} + Z_d n_{d0}. \tag{1}$$

The normalized governing equations are the continuity and momentum equations for positive ions,

$$\frac{\partial n_p}{\partial t} + \frac{\partial}{\partial x}(n_p u_p) = 0, \tag{2}$$

$$\frac{\partial u_p}{\partial t} + u_p \frac{\partial u_p}{\partial x} = -\frac{\partial \phi}{\partial x} - \sigma_p \frac{\partial}{\partial x}\left(\frac{p_p}{n_p}\right) + \eta \frac{\partial^2 u_p}{\partial x^2}, \tag{3}$$

the adiabatic pressure equation for positive ions,

$$\frac{\partial p_p}{\partial t} + u_p \frac{\partial p_p}{\partial x} + \gamma p_p \frac{\partial u_p}{\partial x} = 0, \tag{4}$$

the continuity and momentum equations for cold negative ions,

$$\frac{\partial n_n}{\partial t} + \frac{\partial}{\partial x}(n_n u_n) = 0, \tag{5}$$

$$\frac{\partial u_n}{\partial t} + u_n \frac{\partial u_n}{\partial x} = \beta \frac{\partial \phi}{\partial x}, \tag{6}$$

and the Poisson equation,

$$\frac{\partial^2 \phi}{\partial x^2} = \mu_e n_e - n_p + \mu_n n_n + \mu_d, \tag{7}$$

where n_e is the electron number density.

The electron density follows the Cairns nonthermal distribution [18, 19]:

$$n_e = \left(1 - \alpha\phi + \alpha\phi^2\right) e^{\phi}. \tag{8}$$

Here α is the nonthermal parameter: $\alpha = 0$ recovers the Boltzmann distribution, while larger α indicates a more pronounced population of suprathermal electrons. Physically acceptable values for the Cairns distribution lie in the range $0 \le \alpha \le 4/7$ to ensure the positivity of the electron distribution function [18, 20].

The normalization scheme used throughout is as follows. The number densities are normalized by their respective equilibrium values, $n_s = N_s/N_{s0}$; the fluid velocities $u_s = U_s/C_s$, where $C_s = \sqrt{k_B T_e/m_p}$ is the DIA speed; the electrostatic potential $\phi = e\Phi/(k_B T_e)$; the space coordinate $x = X/\lambda_D$ with $\lambda_D = \sqrt{\varepsilon_0 k_B T_e/(n_{p0} e^2)}$; and time $t = \omega_{pi} T$ where $\omega_{pi} = \sqrt{n_{p0} e^2/(\varepsilon_0 m_p)}$. The dimensionless parameters are $\sigma_p = T_p/T_e$, $\beta = m_p/(Z_n m_n)$, $\mu_e = n_{e0}/n_{p0}$, $\mu_n = Z_n n_{n0}/n_{p0}$, $\mu_d = Z_d n_{d0}/n_{p0}$, and η is the normalized ion viscosity coefficient. The adiabatic index $\gamma = 3$ for one-dimensional motion. The neutrality condition (1) in normalized form is $\mu_e = 1 - \mu_n - \mu_d$.

III. KDV EQUATION AND SOLITION

We have employed the reductive perturbation method (RPM) [8, 9] with the stretched variables

$$\xi = \varepsilon^{1/2}(x - V_p t), \quad \tau = \varepsilon^{3/2} t, \tag{9}$$

where $\varepsilon \ll 1$ is the smallness parameter and V_p is the linear phase velocity. The dependent variables are expanded as

$$n_p = 1 + \varepsilon n_{p1} + \varepsilon^2 n_{p2} + \cdots, \tag{10}$$
$$u_p = \varepsilon u_{p1} + \varepsilon^2 u_{p2} + \cdots, \tag{11}$$
$$p_p = 1 + \varepsilon p_{p1} + \varepsilon^2 p_{p2} + \cdots, \tag{12}$$
$$n_n = 1 + \varepsilon n_{n1} + \varepsilon^2 n_{n2} + \cdots, \tag{13}$$
$$u_n = \varepsilon u_{n1} + \varepsilon^2 u_{n2} + \cdots, \tag{14}$$
$$\phi = \varepsilon \phi_1 + \varepsilon^2 \phi_2 + \cdots. \tag{15}$$

By equating the lowesr-order coefficient, and then substituting and rearranging the first order purturbed quentities n_{p1}, u_{p1}, p_{p1}, n_{n1}, u_{n1}, ϕ_1; one can obtain the dispersion relation

$$\mu_e(1-\alpha) - \frac{\mu_n \beta}{V_p^2} + \frac{1}{V_p^2 - \gamma\sigma_p} = 0, \tag{16}$$

which yields

$$V_p^2 = \frac{-\Lambda \pm \sqrt{\Lambda^2 - 4\mu_e(1-\alpha)\mu_n\beta\gamma\sigma_p}}{2\mu_e(1-\alpha)}, \tag{17}$$

with

$$\Lambda = 1 - \mu_n\beta - \mu_e(1-\alpha)\gamma\sigma_p, \tag{18}$$

The two roots correspond to the fast and slow DIA modes [6, 15]. Throughout this work we focus on the fast mode (upper sign), which has the higher phase speed.

Eliminating the second-order perturbed quantities n_{p2}, u_{p2}, p_{p2}, n_{n2}, u_{n2}, ϕ_2 yields the compatibility condition

$$\frac{\partial \phi_1}{\partial \tau} + A\phi_1 \frac{\partial \phi_1}{\partial \xi} + B\frac{\partial^3 \phi_1}{\partial \xi^3} = 0, \tag{19}$$

which is the KdV equation. The two coefficients are

$$A = \frac{3V_p^4 - 3\mu_n\beta^2(V_p^2 - \gamma\sigma_p)^2 - \mu_e(V_p^2 - \gamma\sigma_p)^3}{2V_p\big[\mu_n\beta(V_p^2 - \gamma\sigma_p)^2 + V_p^2\big]}, \tag{20}$$

$$B = \frac{V_p^3(V_p^2 - \gamma\sigma_p)^2}{2\big[\mu_n\beta(V_p^2 - \gamma\sigma_p)^2 + V_p^2\big]}, \tag{21}$$

The nonlinear coefficient A determines soliton polarity and amplitude; the dispersive coefficient $B > 0$ always resists steepening.

The single-soliton solution in the stationary frame $\zeta = \xi - U\tau$ is

$$\phi(\xi, \tau) = \phi_m \operatorname{sech}^2\left(\frac{\xi - U\tau}{\Delta}\right), \tag{22}$$

with amplitude and width

$$\phi_m = \frac{3U}{A}, \qquad \Delta = \sqrt{\frac{4B}{U}}. \tag{23}$$

The sign of ϕ_m is determined by $\mathrm{sgn}(A)$: compressive ($A > 0$) or rarefactive ($A < 0$) solitons. The soliton speed $U > 0$ is a free parameter [7, 16].

IV. KDV-B EQUATION AND SOLITION

Now applying the RPM [8, 9] and repeat the earlier procedure, with the ion viscosity ordered as $\eta = \varepsilon^{1/2}\eta_0$ one can obtain the dispersion relation for the DIA shocks identical to Eq. (17). Eliminating the second-order perturbed quantities then yields the KdV–Burgers equation as

$$\frac{\partial \phi_1}{\partial \tau} + A\phi_1 \frac{\partial \phi_1}{\partial \xi} + B\frac{\partial^3 \phi_1}{\partial \xi^3} = C\frac{\partial^2 \phi_1}{\partial \xi^2}, \tag{24}$$

The three coefficients are

$$A = \frac{3V_p^4 - 3\mu_n\beta^2(V_p^2 - \gamma\sigma_p)^2 - \mu_e(V_p^2 - \gamma\sigma_p)^3}{2V_p\big[\mu_n\beta(V_p^2 - \gamma\sigma_p)^2 + V_p^2\big]}, \tag{25}$$

$$B = \frac{V_p^3(V_p^2 - \gamma\sigma_p)^2}{2\big[\mu_n\beta(V_p^2 - \gamma\sigma_p)^2 + V_p^2\big]}, \tag{26}$$

$$C = \frac{\eta_0 V_p^2(V_p^2 - \gamma\sigma_p)}{2\big[\mu_n\beta(V_p^2 - \gamma\sigma_p)^2 + V_p^2\big]}. \tag{27}$$

The nonlinear coefficient A in Eq. (25) is exactly same as in Eq. (20) and dispersive coefficient B in Eq. (26) is exactly same as in Eq. (21). The dissipative coefficient C accounts for energy loss through ion viscosity. In the limit $\eta_0 \to 0$ ($C \to 0$), Eq. (24) reduces to the pure KdV equation [6, 7].

When dissipation is the dominant factor $C \gg B$, the dispersive term in Eq. (24) is negligible, and the solution simplifies to the monotonic Burgers shock [10, 11]:

$$\phi(\xi, \tau) = \frac{\phi_m}{2}\left[1 - \tanh\left(\frac{\xi - U\tau}{\Delta}\right)\right], \tag{28}$$

where the amplitude and width can be expressed as

$$\phi_m = \frac{U}{A}, \qquad \Delta = \sqrt{\frac{2C}{U}}. \tag{29}$$

When dispersion and dissipation are comparable ($B \sim C$), oscillatory shock (undulatory shock) solutions are obtained, which interpolate between the soliton and the monotonic shock profiles [12, 17].

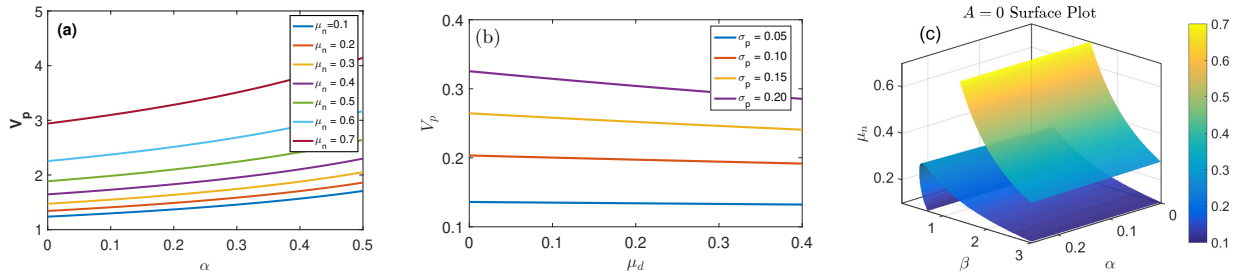


FIG. 1. Phase velocity V_p as a function of (a) the nonthermal parameter α for several μ_n ($\mu_d = 0.15$, $\beta = 0.40$, $\sigma_p = 0.05$, and $\gamma = 3$) and (b) dust number concentration relative to positive ion number density μ_d for several σ_p ($\alpha = 0.1$, $\beta = 0.40$, $\mu_n = 0.25$, and $\gamma = 3$). V_p increases monotonically with both α, μ_n, and σ_p but decreases with higher μ_d, reflecting the weakening of the electrostatic restoring force by energetic electrons and by the reduction of electron density due to dust.(c) The critical surface ($A = 0$) at fixed $\mu_d = 0.15$ and $\sigma_p = 0.05$ defines a bifurcated stability boundary in the (α, β, μ_n) parameter space, where polarity reversal is mainly influenced by μ_n and β, with minimal effect from α, due to the dispersion relation having two roots.

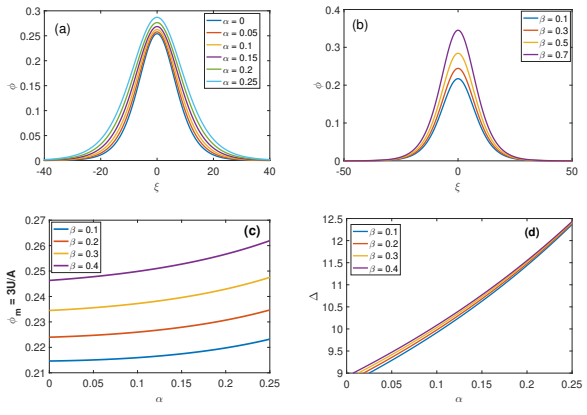


FIG. 2. (a) DIA soliton profiles for various α ($\mu_n = 0.25$,$\mu_d = 0.15$, $\beta = 0.40$, $\sigma_p = 0.05$, $\gamma = 3$, and $U = 0.1$): both amplitude and width increase with α, reflecting the weakening of the nonlinear and dispersive restoring forces by nonthermal electrons. (b) Soliton profiles for various β ($\mu_n = 0.25$,$\mu_d = 0.15$, $\alpha = 0.1$, $\sigma_p = 0.05$, $\gamma = 3$, and $U = 0.1$) show that as β increases, the amplitude and width of the soliton also increase, driving the system toward polarity reversal and widening the soliton. Soliton (c) amplitude ϕ_m and (d) width Δ vs. α for several α and β confermed the earlier statments.

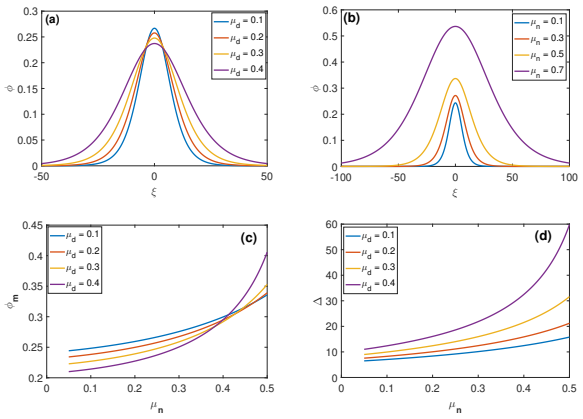


FIG. 3. (a) Soliton profiles for varying μ_d ($\alpha = 0.1$, $\mu_n = 0.25$, $\beta = 0.40$, $\sigma_p = 0.05$, and $\gamma = 3$): lower dust loading narrows and amplifies the soliton by reducing electron shielding efficiency. (b) Soliton profiles for varying μ_n: increasing negative-ion density increases both amplitude and width. (c) ϕ_m vs. μ_n for several μ_d shows that below the a certain value ($\mu_n < 0.4$) amplitude decreases with μ_d but above the value $\mu_n > 0.4$ amplitude increases with μ_d (d) Δ vs. μ_n for several μ_d; the width also increases with both μ_n and μ_d.

V. RESULTS AND DISCUSSION

We have numerically investigated the nonlinear propagation of DIA solitary and shock waves in an unmagnetized, collisionless electronegative dusty plasma containing warm positive ions with adiabatic pressure, cold negative ions, Cairns-distributed nonthermal electrons, and stationary negatively charged dust grains. Unless stated otherwise, the default parameters are chosen as $\alpha = 0.1$, $\mu_n = 0.25$, $\mu_d = 0.15$, $\beta = 0.40$, $\sigma_p = 0.05$, $\gamma = 3$, and $\eta_0 = 0$; for shock-profile calculations, $\eta_0 = 0.5$ is used. These values are aligned with laboratory electronegative dusty plasma discharges and previous studies [6, 7, 14, 16, 17].

Figure 1(a) shows the variation of V_p as a function of the nonthermal parameter α for various values of μ_n. As shown in the figure, an increase in α reduces the effective electron restoring force through the $(1-\alpha)$ factor in the dispersion relation [Eq. (16)], leading to a increase in V_p. This increase is attributed to the larger population of energetic electrons, which enhance the local electrostatic restoring pressure and consequently faster the propagation of the DIA mode. This finding is consistent with the results of Haider [7] and Alinejad [20]. Moreover, an increase in μ_n enhance V_p because the additional inertia of negative ions promot wave propagation. Figure 1(b) shows V_p as a function of the dust concentration μ_d for $\alpha = 0.15$ and $\mu_n = 0.25$. An increase in μ_d decreases the normalized electron density $\mu_e = 1-\mu_n-\mu_d$, which weak-

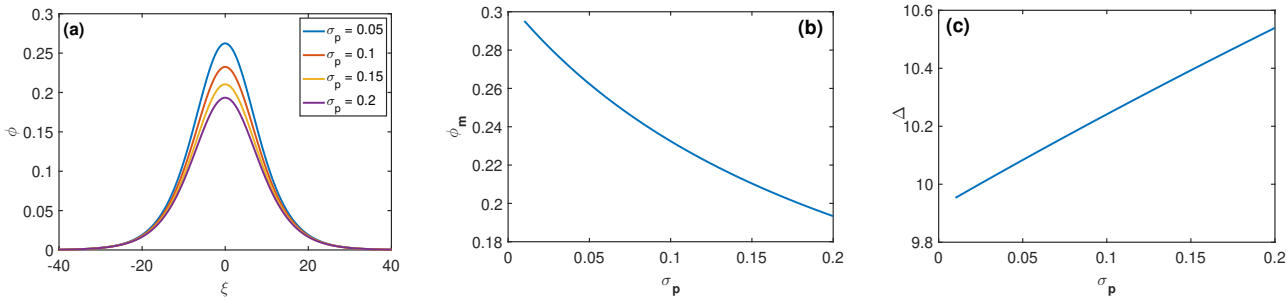


FIG. 4. Effect of positive to negative ion temperature ratio σ_p ($\alpha = 0.1$, $\mu_n = 0.25$, $\mu_d = 0.15$, $\beta = 0.40$, $\gamma = 3$, and $U = 0.1$): (a) soliton profiles showing that warmer positive ions suppress both amplitude and width; (b) ϕ_m vs. σ_p: amplitude decreases monotonically as ion thermal pressure disperses the wave; (c) Δ vs. σ_p: width become widther as σ_p raises.

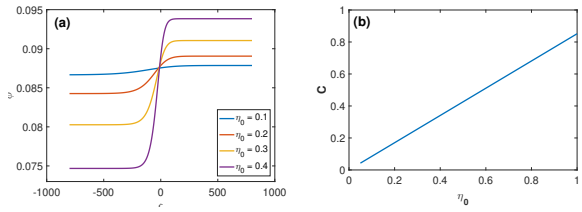


FIG. 5. (a) KdV-B shock profiles for several values of the viscosity parameter η_0 ($\alpha = 0.15$, $\mu_n = 0.20$, $\mu_d = 0.15$, $\beta = 0.50$, $\sigma_p = 0.05$, $\gamma = 3$, $U = 0.1$): small η_0 yields oscillatory shocks; large η_0 yields monotonic tanh-type shocks. The shock front broadens with increasing viscosity. (b) Dissipative coefficient C versus η_0, confirming the linear relationship predicted by Eq. (27).

ens the electron shielding force. Since electron pressure is the primary restoring mechanism for the DIA mode, a decrease in μ_e reduces V_p. This trend has been observed in earlier studies on multi-ion dusty plasmas [6, 11, 15]. In contrast, additional positive-ion thermal pressure enhances the phase velocity.

Figure 1(c) illustrates the $A = 0$ surface plot. Because the underlying dispersion relation admits two roots, this marginal stability condition generates a bifurcated surface in the (α, β, μ_n) space. This analysis focuses on the upper branch of this surface, which is relevant to the regime of interest. In the language of the Sagdeev pseudopotential, such branching is typically associated with two distinct classes of solitary wave solutions, with polarity determined by the sign of the effective potential. For the parameters adopted in this work, the operating point lies entirely below the upper branch of the $A = 0$ surface; therefore, all solitary-wave solutions obtained here are compressive. This outcome is not an artifact of a particular parameter choice but a direct consequence of the constraint imposed by the critical surface on the admissible nonlinear structures throughout the explored region.

Figure 2(a) presents the soliton profile ϕ versus ξ for several values of α, with $\mu_n = 0.25$, $\mu_d = 0.15$, $\beta = 0.40$, $\sigma_p = 0.05$, amd $\gamma = 3$ held fixed. Throughout this range A stays positive but its magnitude increases as α increases, because the growing nonthermal electron population strength the electrostatic restoring force and thus the effective coefficient. Since $\phi_m = 3U/A$ [Eq. (29)], a smaller A at fixed U translates directly into a taller soliton. At the same time, $\Delta = \sqrt{4B/U}$ grows, because B increases as V_p rises with α. The net effect, visible in Fig. 2(c and d), is that solitons become both taller and wider as α increases. This finding is noteworthy: nonthermal electrons promote the formation of large-amplitude, spatially extended DIA solitary structures, aligning with the results of Haider [7] and Misra et al. [12].

A decrease in β, indicating heavier negative ions, increases the effective plasma inertia and decreases V_p [Eq. (17)] which enhances the nonlinear term $\mu_n\beta^2$ in A [Eq. (20)]. This potentially is driving A toward zero and eventually causing a sign change, which transforms compressive solitons into rarefactive solitons. For parameter sets below the critical surface (Fig.1 (c)), both compressive and rarefactive structures emerged as β varied. Furthermore, the dispersive coefficient B increases with β, leading to a wider soliton width (Fig. 2(b and d)). This sensitivity to β has also been documented by Sayed et al. [6] and Haider and Nahar [11] for superthermal electron distributions. As α approaches the critical value α_c where $A \to 0$, the predicted amplitude diverges, signaling that the KdV description is no longer adequate and that a modified KdV or Gardner treatment would be required near this point.

Figures 3(a) show the effect of μ_d on the soliton profile for $\mu_n = 0.25$, $\alpha = 0.15$, $\beta = 0.40$, $\sigma_p = 0.05$, and $\gamma = 3$, all kept fixed. When μ_d increases, the effective electron concentration $\mu_e = 1 - \mu_n - \mu_d$ decreases, and this enhances the dispersive coefficient B; as a result, the soliton width Δ increases with μ_d regardless of the value of μ_n. The amplitude, however, does not follow the same simple pattern. For μ_n below about 0.4, which is the situation shown in Fig. 3 (c), the reduction of μ_e strengthens the term $(\mu_e V_p^2 - \gamma\sigma_p)^3$ appearing in the numerator of A [Eq. (20)]. This causes A to grow with μ_d, so the amplitude $\phi_m = 3U/A$ decreases. Once μ_n rises above roughly 0.4, the further loss of μ_e instead weak-

ens this same term, A then decreases with μ_d, and the amplitude increases in the opposite sense. In this second case, a sufficiently large μ_d can drive A close to zero, marking the onset of rarefactive solitons. This reversal of the amplitude–μ_d dependence around $\mu_n \approx 0.4$, together with the steady broadening of the width, reflects the dual role of μ_d in the dispersion relation, a feature also reported in dusty multi-ion plasmas [6, 7, 16, 24].

The lower panels of Fig. 3 present the amplitude–μ_n and width–μ_n curves. Both ϕ_m and Δ increase steadily with μ_n for the parameters used in this study. From the analytical expression for A [Eq. (20)], raising μ_n lowers μ_e and, at the same time, adds to the negative-ion inertia term $\mu_n\beta^2$. For the present parameter range, these two effects combine to reduce $|A|$ while B increases. Since ϕ_m varies inversely with A and Δ scales with B, the soliton grows both taller and wider as μ_n is increased as can be observed in Fig. 3 (b). Liu et al. reported a similar trend for electronegative plasmas [14], and the same qualitative behaviour is supported by experiments on dusty electronegative plasmas [13] and also by theoretical studies of multi-ion DIA waves [6, 7, 15]. Physically, the negative ions act as an additional charge species that competes with the positive ions in setting the restoring force of the plasma. As μ_n grows, this competition weakens the nonlinearity and strengthens the dispersion, so the soliton emerges correspondingly larger and broader.

Figure 4(a) illustrates the solitary wave profile for different values of σ_p. The positive-ion thermal pressure acts as a secondary restoring force that counteracts the electrostatic focusing of the wave. Increasing σ_p raises V_p through the adiabatic pressure term $\gamma\sigma_p$ in the dispersion relation (17). The changes in A and B lead to reduced ϕ_m but enrich Δ; thus, warmer positive ions produce shorter and wider solitons (Fig. 4). This outcome is anticipated because higher thermal pressure disperses the wave more effectively, preventing the formation of large-amplitude, spatially concentrated structures typical of cold-ion plasmas. Similar behavior was observed by Atteya *et al.* [23] and Haider and Nahar [11].

When the ion viscosity $\eta_0 \neq 0$, the dissipative coefficient C becomes positive, and the KdV-B equation (24) supports shock solutions. Figure 5 (a) presents the shock profile ϕ versus ξ for various values of η_0. As η_0 increases, C increases linearly [Eq. (27) and Fig. 5(b)], resulting in three distinct regimes.

1. *Soliton-like regime* ($C \ll B$): When η_0 is small, the shock front is characterized by oscillations, with dispersive ripples forming behind the main compression. This behavior is similar to that of a weakly damped soliton, where dispersion maintains coherent wave packets despite weak dissipation.

2. *Oscillatory shock regime* ($B \sim C$): At intermediate values of η_0, a distinct oscillatory shock, also known as an undulatory shock, emerges. The amplitude of the leading edge is influenced by both A and C, while the trailing oscillations are primarily determined by B. Such shock structures are frequently observed in laboratory dusty plasma experiments [10, 13].

3. *Monotonic shock regime* ($C \gg B$): For large η_0, dissipation becomes dominant over dispersion, leading to a monotonic shock profile that approaches the *tanh* solution (28). The shock thickness $\Delta = 2C/U$ increases with η_0, as depicted in Fig. 5(a), where the transition region systematically broadens.

Figure 5(b) illustrates the dissipative coefficient C as a function of η_0. The observed linear relationship corroborates the analytical expression (27), indicating that C is directly proportional to η_0 when V_p and σ_p are held constant. The slope is influenced by the plasma composition, specifically through μ_n, μ_d, and β; an increased content of negative ions and a higher concentration of dust both lead to a reduction in the slope, as the denominator of C increases with the inertial terms. The linear scaling of C with η_0 offers a direct observational method. By measuring the shock thickness and ion viscosity, the plasma composition can be inferred using Eq. (27). Similar linear relationships have been documented by Haider and Nahar [11] for superthermal electron models, and by Azad and Haider [17] for charge-fluctuating dusty plasmas. The transition from oscillatory to monotonic shocks serves as a key observational indicator of KdV-B dynamics. In this model, the transition occurs when $\eta_0 \sim B/(C/\eta_0) = B/C_{\text{slope}}$, where C_{slope} represents the coefficient of η_0 in Eq. (27). Since C_{slope} decreases with increasing μ_d or μ_n, larger negative-ion or dust concentrations push this transition toward higher η_0—physically, because both species enhance the dispersive character of the plasma, a correspondingly larger viscosity is then needed to reach the monotonic regime.

These results extend the earlier work of Sayed *et al.* [6] on DIA solitary waves in positive-negative ion dusty plasmas by adding warm positive-ion pressure and Cairns-distributed nonthermal electrons to the model. The polarity-reversal mechanism found here is governed mainly by the competition between the two ion species rather than by electron nonthermality, in agreement with the conclusions reached by Haider [7] for magnetized plasmas, while the influence of Cairns electrons on soliton amplitude and width matches the findings of Alinejad [20] and Habib *et al.* [21]. The three-regime shock behavior identified here—oscillatory, transitional, and monotonic—is consistent with the experimental observations of Nakamura *et al.* [10] and the theoretical analysis of Misra *et al.* [12]. Including warm positive-ion pressure brings σ_p into the model as an independent control parameter, something cold-ion treatments cannot offer: warmer positive ions reduce both the soliton amplitude and width and lower the dissipative coefficient, since they raise $V_p^2 - \gamma\sigma_p$ through their effect on V_p.

VI. CONCLUSIONS

This work has examined the nonlinear dust-ion-acoustic (DIA) solitary and shock waves that arise in an electronegative, unmagnetized dusty plasma containing warm adiabatic positive ions, cold negative ions, Cairns-distributed nonthermal electrons, and stationary negatively charged dust grains. Applying the reductive perturbation method to this four-component system, we derived the KdV equation to study the soliton profile. Than considering the viscuss term η_0 KdV equation is found, from which we have studied the Shock profile.

The principal conclusions are as follows:

1. The phase velocity V_p increases as the nonthermal parameter α, negative-ion concentration μ_n, dust concentration μ_d increase, and higher positive-ion temperature ratio σ_p.

2. The polarity reversal critical surface ($A = 0$) is primarily determined by the competition between positive and negative ions, characterized by the parameters μ_n and β.

3. Both compressive ($A > 0$) and rarefactive ($A < 0$) DIA solitons are supported by the system. An increase in α leads to solitons with larger amplitudes and greater widths, whereas an increase in σ_p results in wider solitons with smaller amplitudes.

4. The shock structure is governed by the ratio B/C. Low viscosity yields oscillatory shocks, whereas high viscosity produces monotonic shocks. The dissipative coefficient C is linearly proportional to η_0, with the proportionality slope dependent on the plasma composition.

5. The present model is applicable to laboratory SF_6-argon discharges, Earth's mesosphere, and Saturn's E-ring, where the coexistence of negative ions, nonthermal electrons, and charged dust is well established.

The results obtained in this study give a more complete picture of nonlinear DIA wave dynamics in dusty electronegative plasmas, since the combined role of nonthermal electrons, negative ions, and charged dust grains has not been fully addressed in earlier three-component models. Because the parameter ranges considered here are close to those reported for the Earth's mesosphere and Saturn's E-ring, the present analysis may help in interpreting the nonlinear electrostatic structures observed in such environments.

Funding Statement: This research received no specific grant from any funding agency.

[1] N. N. Rao, P. K. Shukla, and M. Y. Yu, Planet. Space Sci. **38**, 543 (1990).
[2] P. K. Shukla and V. P. Silin, Phys. Scr. **45**, 508 (1992).
[3] A. Barkan, R. L. Merlino, and N. D'Angelo, Phys. Plasmas **2**, 3563 (1995).
[4] Y. Nakamura and A. Sarma, Phys. Plasmas **8**, 3921 (2001).
[5] P. K. Shukla and A. A. Mamun, *Introduction to Dusty Plasma Physics* (IOP Publishing, Bristol, 2002).
[6] F. Sayed, M. M. Haider, A. A. Mamun, P. K. Shukla, B. Eliasson, and N. Adhikary, Phys. Plasmas **15**, 063701 (2008).
[7] M. M. Haider, Eur. Phys. J. D **70**, 28 (2016).
[8] H. Washimi and T. Taniuti, Phys. Rev. Lett. **17**, 996 (1966).
[9] T. Taniuti and N. Yajima, J. Math. Phys. **10**, 1369 (1969).
[10] Y. Nakamura, H. Bailung, and P. K. Shukla, Phys. Rev. Lett. **83**, 1602 (1999).
[11] M. M. Haider and A. Nahar, Z. Naturforsch. A **72**, 627 (2017).
[12] A. P. Misra, N. P. Acharya, S. Basnet, and R. Khanal, Phys. Plasmas **31**, 093701 (2024).
[13] R. L. Merlino, Plasma Phys. Appl. **81**, 73 (2006).
[14] Z. Liu, Entropy **25**, 1363 (2023).
[15] A. A. Mamun and P. K. Shukla, Phys. Lett. A **372**, 3216 (2008).
[16] Md. A. Salam, M. A. Akbar, M. Z. Ali, and M. M. Haider, Results Phys. **26**, 104376 (2021).
[17] M. H. Azad, M. M. Haider, and O. Rahman, J. Korean Phys. Soc. (2025).
[18] R. A. Cairns, A. A. Mamun, R. Bingham, R. Bostöm, R. O. Dendy, C. M. C. Nairn, and P. K. Shukla, Geophys. Res. Lett. **22**, 2709 (1995).
[19] M. M. Haider Contrib. Plasma Phys. **53**(3), 234 – 244 (2013).
[20] H. Alinejad, Astrophys. Space Sci. **327**, 131 (2010).
[21] K. Habib, M. R. Hassan, M. S. Alam, and S. Sultana, Plasma Phys. Control. Fusion **66**, 065027 (2024).
[22] N. P. Acharya, S. Basnet, and R. Khanal, Phys. Scr. **99**, 035603 (2024).
[23] A. Atteya, S. Sultana, and R. Schlickeiser, Chin. J. Phys. **56**, 1931 (2018).
[24] M. R. Hassan, S. Biswas, K. Habib, and S. Sultana, Results Phys. **33**, 105106 (2022).